Numerical simulation of the large-scale North American monsoon water sources

Michael G. Bosilovich
NASA Data Assimilation Office

Yogesh C. Sud
NASA Climate and Radiation Branch

Siegfried D. Schubert
NASA Data Assimilation Office

Gregory K. Walker
NASA Climate and Radiation Branch

Abstract. A general circulation model (GCM) that includes water vapor tracer (WVT) diagnostics is used to delineate the dominant sources of water vapor for precipitation during the North American monsoon. A 15-year model simulation carried out with one-degree horizontal resolution and time varying sea surface temperature is able to produce reasonable large-scale features of the monsoon precipitation. Within the core of the Mexican monsoon, continental sources provide much of the water for precipitation. Away from the Mexican monsoon (eastern Mexico and Texas), continental sources generally decrease with monsoon onset. Tropical Atlantic Ocean sources of water gain influence in the southern Great Plains states where the total precipitation decreases during the monsoon onset. Pacific ocean sources do contribute to the monsoon, but tend to be weaker after onset. Evaluating the development of the monsoons, soil water and surface evaporation prior to monsoon onset do not correlate with the eventual monsoon intensity. However, the most intense monsoons do use more local sources of water than the least intense monsoons, but only after the onset. This suggests that precipitation recycling is an important factor in monsoon intensity.

1. Introduction

The North American monsoon provides much of the water for Mexico and the southwestern Untied States (Douglas et al. [1993]). Many studies have strived to identify the source(s) of water for the North American monsoonal precipitation to better understand the dynamical and hydrological processes (e.g. *Hales et al.* [1974], *Adams and Comrie* [1997] and *Higgins et al.* [1997]). In general, this is accomplished by evaluating large-scale synoptic fields (geopotential height, wind and moisture) along with the hydrologic budget (precipitation, evaporation and moisture transport). Early studies generally focused on the monthly mean fields, and more recently diurnal cycles have been studied (*Berbery* [2001]). However, simply examining the flow of moist air and precipitation does not yield much quantitative information about the source of water. For example, moist air that moves from the Gulf of Mexico into the southern United States can be said to come from the Gulf of Mexico, but there is generally no detailed information on how much water evaporated from the Gulf of Mexico, and how much passed over the gulf from some more distant region. Such a detailed delineation of water

sources is vital in characterizing the influence of local and remote sources of water in monsoonal systems.

The North American Monsoon system has several distinct regions of interest. At small spatial scales (e.g. sea breeze and gulf surges), the Gulf of California can have a profound impact on local circulation and moisture fields. At larger spatial scales (500 Km), the onset of the monsoon is characterized by a substantial increase in precipitation over western Mexico (extending northward to Arizona and New Mexico) with a concurrent decrease of precipitation over eastern Mexico and extending to Texas (*Douglas et al.* [1993], *Barlow et al.* [1998]). In the southern Great Plains of the United States, the Low-Level Jet (LLJ) and associated moisture transport are generally unchanged with monsoon onset, but precipitation related to the LLJ decreases (*Higgins et al.* [1997]). The southwestern United States has been the focus of a number of studies on sources of water for monsoonal precipitation, though these have been mostly concerned with oceanic sources of water, namely the Gulf of California versus the Gulf of Mexico (*Schmitz and Mullen* [1996]). Continental sources of water are generally not evaluated, because extensive observations of evaporation and surface wetness are not readily available.

While continental evaporation occurs over a smaller area compared to the vast oceans, evapotranspiration directly contributes to water vapor and moist static energy within the planetary boundary layer (*Bosilovich* [2002]). Recent studies are beginning to consider the implications of local continental evaporation feedback on the North American monsoon. *Anderson and Roads* [2001], for example, suggest that the atmosphere 700 HPa and above is generally divergent and therefore less conducive to forming condensation from remote sources such as the Gulf of Mexico during the monsoon. The most prominent low-level sources are then water from the Gulf of California and local evaporation. *Small* [2001] simulations identified an evaporative feedback of surface wetness on monsoon precipitation in a mesoscale model. Idealized soil wetness anomalies were imposed (as in typical sensitivity experiments), and the feedback process has been discussed in many studies (e.g. *Eltahir and Bras* [1996] and *Bosilovich and Sun* [1999 a and b])

Koster et al. [1986] and *Jousaume et al.* [1986] used passive tracers in a GCM to simulate regional sources of water and their movement, independent of all other geographical sources. Using this methodology, diagnostic data can quantify the integrated path that water follows to get from a source region (initiated as evaporation) to a destination (as precipitation). This methodology, termed Water Vapor Tracers (WVT), quantifies the local and remote sources of precipitation, and precipitation recycling (under certain conditions) (*Bosilovich and Schubert* [2002]). Simpler precipitation recycling diagnostics can determine the local source of water for precipitation, but cannot identify the geographic source region of remote sources of water (*Brubaker et al.* [1993], *Bosilovich and Schubert* [2001]).

In the present study, our motivation was to characterize the development and maintenance of the North American monsoon by delineating the sources of water vapor for precipitation. We have simulated the climate for 15 years with

a general circulation model (GCM) that includes WVT diagnostics tailored to quantify the geographic sources of water for the North American monsoon. In particular, we focus on the large-scale (regions, continents and oceans) sources of water and the large-scale circulation involved in the precipitation in Mexico and in the southern Great Plains states. In the next section, we discuss the atmospheric GCM and arrangement of the WVTs. The WVTs are a diagnostic tool that provides quantitative evaluation of geographical sources of water. We provide a brief discussion of the WVT formulation, referring the reader to *Bosilovich and Schubert* [2002] for more details. Section 3 validates the large-scale hydrologic data from the model with observations and the NCEP/NCAR 50-year reanalysis (*Kalnay et al.* [1996], *Kistler et al.* [2001]). In section 4, we examine the large-scale geographic sources of water for monsoonal precipitation, focusing on the onset of the monsoon.

2. Model and Methodology

The atmospheric numerical model used in this study is called the Finite Volume General Circulation Model (FVGCM). The atmospheric dynamics are based on the flux form semi-Lagrangian advection scheme (*Lin and Rood* [1996, 1997]). The dynamical core was developed at Goddard Space Flight Center, but is also included in the National Center For Atmospheric Research (NCAR) community model (*Collins et al.* [2002]). The atmospheric physics are from the NCAR Community Climate Model version 3 (CCM3) including the convection, radiation, boundary layer and land surface parameterizations (*Kiehl et al.* [1998] and *Bonan* [1998]). The climate and atmospheric circulation of the FVGCM are described by *Chang et al.* [2001]. Here, we will specifically validate and discuss certain aspects of the model hydroclimatology that pertain to the North American monsoon.

The Water Vapor Tracers (WVTs) have been implemented following *Bosilovich and Schubert* [2002]. Conceptually, a WVT is a passive global atmospheric constituent, and is entirely separate from the model's water vapor variable that interacts with radiation and convection. The source for the WVT is surface evaporation from a limited region of the globe. The WVT is affected by all the processes that act on the water vapor including advection, convection, and boundary layer processes. Advection acts directly on the tracer field. On the other hand, convection acts on the WVT amount in proportion to the total water. For example, if a certain amount of water vapor is condensed, the amount of condensed tracer is assumed to be in proportion of tracer water to total water. In this way, we can compute the amount of precipitation that falls in one region, as a direct result of evaporation in another region or from within the same region. This is a conceptually straightforward approach, but can be computationally expensive as the number of tracers grows. A more detailed discussion about the computation of the tracer tendencies is provided by *Bosilovich and Schubert* [2002].

In this study, we have run the FVGCM for the period 1982 – 2000 with observed weekly SSTs (*Reynolds and Smith* [1994]). The first four years have been discarded to allow for spin up of the circulation. The spatial resolution of the model

is 1.0°×1.25° with 32 vertical levels. We have defined 22 WVTs, and their source regions are shown in Figure 1. Eleven WVTs are identified as large-scale tracers (Figure 1a), which account for continents and oceans that are distant from the region of interest. The other WVTs are identified as regional tracers associated with the North American monsoon (Figure 1b). These generally have a smaller area, but are in close proximity to the region of interest, and may be subject to more subtle variations in the transport of water. Furthermore, these delineate potentially important sources of water vapor, including the Gulf of Mexico and the Pacific Ocean near the west coast of Mexico (called Baja Oceanic). In order to minimize the number of WVTs, some regions were combined for efficiency, such as the north and south polar latitudes, and the Asian and Australian continental sources. Large inland bodies of water were also included with the Polar tracer, because their effects should be more local and the Polar evaporation should not be very large.

3. Validation

Figure 2 shows the FVGCM simulated summertime precipitation and total precipitable water compared with observations. In general, the simulated total precipitable water (TPW) is qualitatively comparable to NASA's water vapor project (NVAP) observations. However, the modeled TPW in the western United States is slightly less than the observations. Also, the observations show a ridge of high precipitable water content over the Gulf of California. This ridge is not well represented in the model simulation; at one-degree resolution, the gulf is not resolved. The simulated precipitation in the central United States is larger than observed and the central maximum is shifted a couple hundred kilometers westward. In general, the simulated precipitation is larger than the observations everywhere, especially in Canada and western Mexico. Such an overestimate of precipitation appears to be a problem common to many GCMs (*Boyle* [1998]).

As discussed previously, the onset of the North American monsoon can be characterized by the difference of June and July monthly precipitation. In western Mexico, the precipitation is significantly increased in July while in eastern Mexico and Texas, precipitation is decreased. Figure 3 compares the difference of June and July observed precipitation (*Higgins et al.*, [1996]), along with the FVGCM simulated and reanalysis (*Kalnay et al.* [1996], *Kistler et al.* [2001]) precipitation and evaporation. The precipitation differences are all comparable. The gauge data do not show as strong an increase of precipitation in the southeastern United States, as the model and reanalysis. However, in the monsoon region (western Mexico and Texas), the model appears to have some veracity in reproducing the characteristics of the monsoon onset precipitation. The evaporation in the FVGCM (Figure 3d) and NCEP Reanalysis (Figure 3e) seem to be correlated with the precipitation differences.

4. Sources of Water

4.1. Monthly Variations

Here, we will use the WVTs to diagnose the fraction precipitation that originates as evaporation from predetermined regions. Figure 4 shows the monthly mean precipitation in and around Mexico that originated as evaporation from the Mexico (MX), Baja Oceanic (BO) and Gulf of Mexico (GM) regions (see Figure 1). In June, water that evaporates from MX is transported into the United States as far north as the central plains where it precipitates. In July, the extent of the MX precipitation is greatly reduced (especially over the central plains states), but the amount is increased over western Mexico. The precipitation in western Mexico from BO increases from June to July, doubling in some places. Also, the water that crosses the Sierra Madre from the Gulf of Mexico increases noticeably in July. *Bosilovich and Schubert* [2002] show the WVT precipitations are generally correlated positively to total precipitation. In other words, when larger than average precipitation occurs, larger than average WVT precipitation occurs. Therefore, it is not surprising that these predominant sources of water vapor all increase (or decrease) in association with a precipitation anomaly. However, we can also determine how the dominant water vapor sources change with respect to precipitation. Figure 5 shows the July minus June percent of precipitation from MX, BO and the sum of tropical sources (GM, CB and Tat). The fraction of precipitation from MX decreases by 10% in eastern Mexico. However, in western Mexico, where the total precipitation increases substantially, the change in MX water vapor fraction is relatively small (Figure 5a). In eastern Mexico, the contribution from the tropical sources increases by more than 15% over a large portion of the area where total precipitation decreases from June to July (Figure 3b). The contribution of the tropical sources to western Mexico also increases (by less than 10%). Generally, over continental Mexico the fractional contribution from BO decreases (5 – 10 %). While the BO precipitation does increase into July, other sources increase more than BO does, thereby reducing the fraction of BO after monsoon onset.

To further investigate the changes during onset, we explore time series of area average sources of water. Figure 6 shows the area of regions labeled TX (Texas) and WMX (Western Mexico), where we area average the WVTs to focus on the key onset regions identified by the precipitation (Figure 3). The mean annual cycle of the major sources of water for precipitation in TX and WMX are shown in Figure 7. In TX, the largest sources of water during June and July are the Gulf of Mexico and Tropical Atlantic Ocean (Tat). While the Tat source shows a seasonal increase between March and August, the GM source increases abruptly (departing from a smooth seasonal cycle) from June to July. The major continental sources, SP and MX, decrease from June into July. During July, the local continental sources are providing less water than in June for precipitation in the TX region. At the same time, a larger fraction of the precipitation originated in GM and Tat in July compared to June. Because the net change of precipitation is negative (Figure 3), the local continental contribution change is positively correlated to the total precipitation change.

In WMX, the major contributor to June and July precipitation is the local continental source (MX, Figure 7b). The major oceanic sources, BO, NPa and Tat, follow a

seasonal cycle, where the circulation changes dramatically but smoothly from May to August, allowing more water from the tropical Atlantic to contribute to WMX than BO or NPa. To further investigate the relationships between the different sources of water and the onset of the monsoon, we evaluate finer time resolution in the next section.

4.2. Pentad Time Series

Data from June and July were averaged into 12 pentads, beginning on June 3 and ending on July 28. The monsoon in WMX appears in the 18 June pentad, which is comparable to *Higgins et al.* [1999] (their Figure 12). However, the range of onset is from 8 June to 3 July, which is smaller than the *Higgins et al.* [1999] observed range (22 May – 12 July).

In order to investigate the mean onset over the fifteen years of simulation, we created a composite of the data, centering each year about the onset of the monsoon. We define pentad day 0 as last pentad before monsoon precipitation occurs in WMX. A composite time series for WMX and TX was created about the pentad day 0. Figure 8 shows the time series of the composite model data for WMX and TX. By design, WMX precipitation increases sharply with onset. In the four pentads prior to onset, WMX averages 1.6 mm day^{-1} and TX averages 3.0 mm day^{-1} precipitation, while in the four pentads after onset, WMX averages 5.2 mm day^{-1} and TX averages 2.2 mm day^{-1} precipitation. TX precipitation does decrease following the onset, but it is the beginning of a trend that continues until pentad day 20. Likewise, WMX evaporation increases sharply after onset, while TX evaporation decreases gradually in time. In WMX, the soil wetness gradually increases after monsoon onset with precipitation. In contrast, TX soil wetness gradually decreases over the whole period.

Most of the TX quantities change gradually across the onset in WMX (Figure 8). However, an exception is total precipitable water (TPW). In both WMX and TX, the TPW increases sharply following monsoon onset. The 850 hPa specific humidity follows a similar pattern, but this is less evident with the near surface specific humidity. In TX, it is unlikely that the TPW increase is related to local evaporation. However, taking less water away by precipitation may leave water in the column. It may also be possible that the atmospheric circulation has brought a warmer wetter air mass to both TX and WMX coincident with the monsoon onset.

Before the onset of the monsoon, both MX and BO are the principal sources of moisture in WMX (Figure 9a). After onset, the MX source increases slightly, while the BO fraction decreases sharply. The actual amount of water provided from BO more than doubles after onset, but this is a smaller increase, compared to the increase of MX (1.9 mm day^{-1} after onset) and Tat, leading to the BO decrease in percent contribution. After onset, the tropical Atlantic Ocean (sum of TAt, CB and GM) provides 1.6 mm day^{-1} of precipitation while the Pacific Ocean (BO plus NPa) provides 1.0 mm day^{-1}. It is also worthwhile to reiterate that the model does not resolve the Gulf of California, which should influence the sources of water. However, the role of the Gulf of California as a source of water may be small, simply because of its small spatial extent, and its importance may be more related to its

impact on the dynamics and smaller scale circulations (not resolved here).

The TX pentad moisture sources show a steady increase of Tat and GM percentages with time (Figure 9b). At the same time, the continental source (MX and SP) percentages are decreasing. All the major sources show a decrease of precipitation following the onset (Figure 9d). While Tat and GM decrease slightly, MX is cut by more than half. This indicates that the reduction in surface evaporation is acting to reduce the precipitation.

4.3. Mexican Monsoon Intensity

In the previous analysis, continental sources of water for the Mexican monsoon (MX in particular) are influential throughout June and July. It seems reasonable to hypothesize that soil water or local evaporation may be predictors of the intensity of the monsoonal precipitation. In other words, more surface soil water or evaporation leads to more MX sources of water and a more intense monsoon. From the pentad data, we determine the three years with most monsoon precipitation (wettest years) and three years with least monsoon precipitation (driest years) in the simulation by averaging the composite precipitation over Pentad Days 5 – 20 in each year of simulation. Figure 10a shows the time series of pentad precipitation for the 15-year average, the three-year average of the wettest monsoons, and the three-year average of the driest monsoons. The wettest monsoons tend to have above average precipitation through most of the period, while the driest monsoon years always produce less than average. Evaporation and soil wetness time series tend to track similar to the precipitation (Figure 10 b and c). There is little difference in the soil moisture early in the period. Also, both the wettest and driest monsoons have evaporation less than average in the first pentad (June 3). The inference is that the local surface water does not make a good predictor of the intensity of the Mexican monsoon.

Higgins et al. [1999] related wet monsoons in southwest Mexico with La Nina and dry monsoons with El Nino SST anomalies. The relationship was explained by the contrasting land/sea surface temperatures. *Castro et al.* [2001] correlated the occurrence of more (less) intense monsoons with cold (warm) SSTs in the eastern North Pacific Ocean and Tropical Pacific Ocean. These are also associated with distinct upper atmosphere circulation patterns. In the model simulation, the wettest years correspond to SSTs from 1987, 1990 and 1999, while the driest years correspond to SSTs from 1991, 1997 and 1998. The SST anomalies leading up to the monsoon for the wet and dry years are presented in Figure 11 a and b. The wet years are not all correlated to any phase of ENSO, but the eastern North Pacific sea surface temperatures are biased cold. The dry years are all related to warm phase of ENSO in the tropics, and the eastern North Pacific SSTs are warm. The wet years show increased heights over the monsoon region, but t-test statistics do not indicate significance (Figure 11c). The dry years have lower heights over the north western United States which leads to increased westerly flow over the monsoon region (Figure 11d). In general, these patterns agree with the conceptual model of monsoon – SST relationship put forth by

Castro et al. [2001], though the wet years are not as robust as the dry years. While the small number of years affects the average, the general features are remarkably similar. Further, the warm SSTs are driving convection and increased TPW along the equator during dry years (Figure 11f). The drier TPW near Mexico is likely related to subsidence. There is a distinct impact on atmospheric moisture transport (Figure 12). In wet years, there appears to be an intensification of the sub tropical Bermuda high associated with stronger easterly flow over Mexico and the Gulf of Mexico. However, the significance of the change seems small especially over the monsoon region. During dry years, there is an increase in westerly flow from the Pacific Ocean, which moves the drier air mass toward the continent (Figure 11f).

This can be discussed further in terms of WVTs and the sources of water for the monsoon. Figure 13 shows the pentad time series of the dominant sources of water for WMX, including the wettest and driest years. In the driest years, BO and NPa sources dominate before the monsoon onset, while Tat sources are less than the mean. Early in the period, there are few discernible differences between the wettest cases and the average cases. NPa sources are slightly less than average early in the period, and BO sources are less than average when the precipitation (Figure 10a) is largest. The MX continental source is somewhat incoherent early in the season. However, following the onset of the monsoon, the wettest cases show larger MX sources than the driest cases (Figure 13a). This implies that prior to the onset, the precipitation is driven by the atmospheric circulation and remote sources of water, and after onset, convective precipitation derives significant water from local continental sources. A positive feedback of local water, which amounts to precipitation recycling, contributes to the monsoonal precipitation. Of course, the local processes cannot be entirely disassociated from the large-scale atmospheric forcing.

5. Summary and Conclusions

The sources of water for North American monsoon precipitation are quantified in a 15-year numerical simulation of the atmospheric circulation. The Finite Volume GCM is capable of reproducing the large-scale characteristics of the monsoon onset and some of the monsoon characteristics related to sea surface temperature forcing. In western Mexico, the major sources of water prior to the monsoon onset are the Pacific Ocean (including near the coast of the Baja peninsula) and the Mexican continental evaporation. Following the monsoon onset, the dominant sources of monsoon precipitation in Mexico are local continental evaporation and transport from the tropical Atlantic Ocean (including the Gulf of Mexico and Caribbean Sea), while the Pacific Ocean sources play a lesser role. Continental sources of water in eastern Mexico and Texas tend to decrease with the seasonal reduction of soil wetness and evaporation. While tropical Atlantic Ocean sources become more important (and total column water increases) throughout the region, the southern Great Plains precipitation still decreases, indicating the importance of continental evaporation to the precipitation.

The intensity of the simulated monsoon is related to the sea surface temperature, consistent with observational analysis. The driest monsoons are related to the warm phase of ENSO, and the wettest monsoons are related to cold SSTs in the northeastern Pacific Ocean. However, the variability of the atmospheric circulation and in the SSTs in the limited number of wet cases is large. The simulated wettest monsoons have larger local continental sources while the drier monsoons have less local sources of precipitation. This suggests that a positive feedback between surface evaporation and monsoon precipitation contributes to the maintenance of the monsoon. However, this is more than a local or columnar process, as the atmospheric circulation differs for the wet and dry monsoons. The degree of soil wetness and evaporation prior to the monsoon onset did not relate to the eventual intensity of the simulated monsoon. Use of water vapor tracer diagnostics in this numerical simulation has permitted the quantification of the effect of local continental evaporation on the water balance in this numerical experiment; this was accomplished without perturbing the environment as in typical "what if" sensitivity studies.

Acknowledgments. This work was partially supported by the NASA/NOAA GAPP/PACS Warm Season Precipitation Initiative and the NASA Global Water and Energy Cycle program.

References

Adams, D. K. and A.C. Comrie, The North American Monsoon, *Bull. Amer. Met. Soc., 78*, 2197 – 2213, 1997.

Anderson, B T., and J. O. Roads, Summertime moisture divergence over the southwestern US and northwestern Mexico, *Geo. Res. Let., 28*, 1973 - 1976, 2001.

Barlow, M., S. Nigam and E. H. Berbery, Evolution of the North American monsoon system, *J. Climate, 11*, 2238 – 2257, 1998.

Berbery, E. H., Mesoscale moisture analysis of the North American monsoon, *J. Clim., 14*, 121 – 137, 2001.

Boyle, J. S., Evaluation of the annual cycle of precipitation over the United States in GCMs: AMIP simulatations, *J. Clim., 11*, 1041-1055, 1998.

Bonan, G. B., The land surface climatology of the NCAR land surface model coupled to the NCAR Community Climate Model, *J. Clim., 11*, 1307 – 1326, 1998.

Bosilovich, M. G., On the Vertical Distribution of Local and Remote Sources of Water for Precipitation. *Meteorol. Atmos. Phys., 80*, 31-41, 2002.

Bosilovich, M. G., and W.-Y. Sun, Numerical simulation of the 1993 Midwestern flood: Land-atmosphere interactions, *J. Clim., 12*, 1490-1505, 1999a.

Bosilovich, M. G. and W.-Y. Sun, Numerical Simulation of the 1993 Midwestern Flood: Local and Remote Sources of Water, *J. Geophys. Res., D 104*, 19415-19424, 1999b.

Bosilovich, M. G., and S. D. Schubert, Precipitation recycling in the GEOS-1 data assimilation system over the central United States, *J. Hydromet., 2*, 26 – 35, 2001.

Bosilovich M. G. and S. D. Schubert, Water vapor tracers as diagnostics of the regional hydrologic cycle, *J. Hydromet., 3*, 149-165, 2002.

Brubaker, K. L., D. Entekahabi and P. S. Eagleson, Estimation of precipitation recycling, *J. Clim.*, 6, 1077-1089, 1993.

Castro, C. L., T. B. McKee, and R. A. Pielke, The relationship of the North American Monsoon to tropical and north Pacific sea surface temperatures as revealed by observational analyses, *J. Clim., 14*, 4449 – 4473.

Chang, Y., S. D. Schubert, S.-J. Lin, S. Nebuda and D.-W. Shen, The climate of the FVCCM-3 Model, NASA/TM-2001-104606, vol. 20, pp. 127, 2001.

Collins, W. D., J. J. Hack, B. A. Boville, P. J. Rasch, D. L. Williamson, J. T. Kiehl, B. Brieglib, C. Bitz, S.-J. Lin, and R. B. Rood, Description of the NCAR Community Atmosphere Model (CAM2), *NCAR/TN In Preparation*, 2002.

Douglas, M. W., R. A. Maddox, K. Howard, and S. Reyes, The Mexican Monsoon, *J. Clim., 6,* 1665-1677, 1993.

Eltahir, E. A. B., and R. L. Bras, Precipitation recycling, *Rev. of Geophysics*, *34*, 367 – 378, 1996.

Hales, J. E., Southwestern United States summer monsoon source – Gulf of Mexico or Pacific Ocean?, *J. Appl. Meteor., 13*, 331 – 342, 1974.

Higgins, R. W., J. E. Janowiak, and Y. Yao, A gridded hourly precipitation data base for the United States (1963–1993), Climate Predictions Center Atlas 1, National Centers for Environmental Prediction, 47 pp., 1996.

Higgins, R. W., Y. Yao, E. S. Yarosh, J. E. Janowiak and K. C. Mo, Influence of the Great Plains low-level jet on summertime precipitation and moisture transport over the central United States, *J. Clim., 10,* 481 – 507, 1997.

Higgins, R. W., Y. Chen, and A. V. Douglas, Interannual variability of the North American warm season precipitation regime, *J. Clim., 12*, 653 – 680, 1999.

Joussaume, S., R. Sadourny and C. Vignal, Origin of precipitating water in a numerical simulation of July climate, *Ocean-Air Interactions*, *1*, 43 – 56, 1986.

Kalnay, E. and coauthors, The NCEP/NCAR 40-year reanalysis project, *Bull. Amer. Meteor. Soc., 77*, 437-471,1996.

Kiehl, J. T., J. J. Hack, G. B. Bonan, B. A. Boville, D. L. Williamson, and P. J. Rasch, The National Center for Atmospheric Research Community Climate Model (CCM3), *J. Clim., 11*, 1131-1149, 1998.

Kistler, R. and coauthors, The NCEP-NCAR 50-year reanalysis: monthly means CD-ROM and documentation, Bull. Amer. Met. Soc., 82, 247 – 267, 2001.

Koster, R. D., J. Jouzel, R. Suozzo, G. Russell, W. Broecker, D. Rind, and P. Eagleson, Global sources of local precipitation as determined by the NASA/GISS GCM, *Geophys. Res. Let., 13*, 121-124, 1986.

Lin, S.-J., and R. B. Rood, Multidimensional flux form semi-lagrangian transport schemes, *Mon. Wea. Rev.*, 124, 2046 – 2070, 1996.

Lin, S.-J., and R. B. Rood, An explicit flux-form semi-Lagrangian shallow-water model on the sphere, *Q. J. Roy. Meteor. Soc., 123*, 2477 – 2498, 1997.

Reynolds, R. W. and T. M. Smith, Improved global sea surface temperature analyses using optimum interpolation, *J. Clim., 6*, 929 – 948, 1994.

Schmitz, J. T. and S. L. Mullen, Water vapor transport associated with the summertime North American monsoon as depicted by ECMWF analyses, *J. Clim., 9*, 1621-1634, 1996.

Simpson, J. J., J. S. Berg, C. J. Koblinsky, G. L. Hufford and B. Beckley, The NVAP global water vapor data set: independent cross comparison and multi year variability, *Remote Sens. Environ., 76*, 112-129, 2001.

Small, E. E., The influence of soil moisture anomalies on variability of the North American monsoon system, Geo. Res. Let., 28, 139 – 142, 2001.

Xie, P., P. A. Arkin, Global Precipitation: A 17-Year Monthly Analysis Based on Gauge Observations, Satellite Estimates, and Numerical Model Outputs, *Bull. Amer. Meteor. Soc., 78*, 2539–2558, 1997

Michael G. Bosilovich and Siegfried D. Schubert, Data Assimilation Office, NASA/GSFC Code 910.3, Greenbelt, MD, 20771. (email: mikeb@dao.gsfc.nasa.gov)

Yogesh Sud and Gregory K. Walker, Climate and Radiation Branch, NASA/GSFC Code 913, Greenbelt MD, 20771.

(Received xx xx, xxxx; revised xx xx, xxxx;
accepted xx xx, xxxx.)

Paper number xx.
xx$09.00

Paper number xx.

Paper number xx.

****Provide running head (45 character max for short title):**

BOSILOVICH ET AL.: LARGE-SCALE N. A. MONSOON

Figure 1. Map showing (a) the large-scale continental and oceanic sources of water, and (b) the North American regional sources of water. The large-scale sources are NPa – north Pacific Ocean, Spa – south Pacific Ocean, Sat – south Atlantic Ocean, InO – Indian Ocean, Tat – Tropical Atlantic Ocean, Nat – north Atlantic Ocean, Eur – Europe, Asa – Asia and Australia, Sam – South America, Afr – Africa and Pol – Polar. The regional sources are SE – South East, SP – Southern Plains, SW – South West, NW – North West, NP – Norhtern Plains, NE – North East, CA – Canada, MX – Mexico, BO – Baja Oceanic, CB – Caribbean Sea, and GM – Gulf of Mexico.

Figure 1. Map showing (a) the large-scale continental and oceanic sources of water, and (b) the North American regional sources of water. The large-scale sources are NPa – north Pacific Ocean, Spa – south Pacific Ocean, Sat – south Atlantic Ocean, InO – Indian Ocean, Tat – Tropical Atlantic Ocean, Nat – north Atlantic Ocean, Eur – Europe, Asa – Asia and Australia, Sam – South America, Afr – Africa and Pol – Polar. The regional sources are SE – South East, SP – Southern Plains, SW – South West, NW – North West, NP – Norhtern Plains, NE – North East, CA – Canada, MX – Mexico, BO – Baja Oceanic, CB – Caribbean Sea, and GM – Gulf of Mexico.

Figure 2. Summer mean (June, July and August) comparison of simulated hydrologic data with observations for FVGCM total precipitable water (cm) (a), precipitation (mm day^{-1}) (b) and observed total precipitable water (c) and observed precipitation (d). TPW observations are from NASA's Water Vapor Project (NVAP; Simpson et al. 2001) for the period 1988 - 1993 and precipitation observations are from Xie and Arkin (1997) for the period 1986-1998. Only model data that overlaps existing observations are included in (a) and (b).

Figure 2. Summer mean (June, July and August) comparison of simulated hydrologic data with observations for FVGCM total precipitable water (cm) (a), precipitation (mm day^{-1}) (b) and observed total precipitable water (c) and observed precipitation (d). TPW observations are from NASA's Water Vapor Project (NVAP; Simpson et al. 2001) for the period 1988 - 1993 and precipitation observations are from Xie and Arkin (1997) for the period 1986-1998. Only model data that overlaps existing observations are included in (a) and (b).

Figure 3. Difference of June and July monthly means for (a) NCDC gage precipitation (*Higgins et al.* [1996]), (b) FVGCM precipitation, (c) NCEP reanalysis precipitation, (d) FVGCM surface evaporation and (e) NCAR reanalysis evaporation. Units are mm day^{-1}. The FVGCM data are for times overlapping the NCDC available data, while NCAR reanalysis are climate averages for the 50-year reanalysis.

Figure 3. Difference of June and July monthly means for (a) NCDC gage precipitation (*Higgins et al.* [1996]), (b) FVGCM precipitation, (c) NCEP reanalysis precipitation, (d) FVGCM surface evaporation and (e) NCAR reanalysis evaporation. Units are mm day^{-1}. The FVGCM data are for times overlapping the NCDC available data, while NCAR reanalysis are climate averages for the 50-year reanalysis.

Figure 4. Precipitation that occurs from MX evaporation in (a) June and (b) July, from BO evaporation in (c) June and (d) July and from GM evaporation in (e) June and (f) July. Units are mm day^{-1}. (a) – (d) are contoured every 0.5 mm day^{-1} with an extra 0.3 mm day^{-1} contour in bold. (e) and (f) are contoured every 0.2 mm day^{-1}.

Figure 4. Precipitation that occurs from MX evaporation in (a) June and (b) July, from BO evaporation in (c) June and (d) July and from GM evaporation in (e) June and (f) July. Units are mm day-1. (a) – (d) are contoured every 0.5 mm day-1 with an extra 0.3 mm day-1 contour in bold. (e) and (f) are contoured every 0.2 mm day-1.

Figure 5. Difference, from June to July, of percent contribution of WVTs to total precipitation for (a) MX, (b) the sum of GM, Tat and CB, and (c) BO. The percent contribution

for each WVT is computed as the sum of monthly ratio over all years.

Figure 5. Difference, from June to July, of percent contribution of WVTs to total precipitation for (a) MX, (b) the sum of GM, Tat and CB, and (c) BO. The percent contribution for each WVT is computed as the sum of monthly ratio over all years.

Figure 6. Map indicating the area where data are averaged for the western Mexico (WMX) and Texas (TX) regions.

Figure 6. Map indicating the area where data are averaged for the western Mexico (WMX) and Texas (TX) regions

Figure 7. Mean annual cycles of the percent contribution of major source regions for precipitation in (a) TX and (b) WMX. Percentages are computed for each month of the simulation then time averaged.

Figure 7. Mean annual cycles of the percent contribution of major source regions for precipitation in (a) TX and (b) WMX. Percentages are computed for each month of the simulation then time averaged.

Figure 8. Composite of pentad data around the onset of heavy precipitation in WMX. The solid curve indicates WMX, and the dashed curve indicates TX. The solid vertical line indicates the time of monsoon onset in WMX.

Figure 8. Composite of pentad data around the onset of heavy precipitation in WMX. The solid curve indicates WMX, and the dashed curve indicates TX. The solid vertical line indicates the time of monsoon onset in WMX.

Figure 9. WVT data before and after WMX monsoon onset. Composite time series of percent of total precipitation for the major water sources in (a) WMX and (b) TX. WVT precipitation amounts of the major water sources before and after WMX monsoon onset for (c) WMX and (d) TX.

Figure 9. WVT data before and after WMX monsoon onset. Composite time series of percent of total precipitation for the major water sources in (a) WMX and (b) TX. WVT precipitation amounts of the major water sources before and after WMX monsoon onset for (c) WMX and (d) TX.

Figure 10. Time series of pentad average (a) precipitation, (b) evaporation and (c) soil wetness (fraction of saturation). The solid line indicates the average of all fifteen years of the simulation, the long dash line indicates average over the three wettest years and the short dash line indicates average over the three driest years.

Figure 10. Time series of pentad average (a) precipitation, (b) evaporation and (c) soil wetness (fraction of saturation). The solid line indicates the average of all fifteen years of the simulation, the long dash line indicates average over the three wettest years and the short dash line indicates average over the three driest years

Figure 11. June surface temperature anomalies for (a) wettest three monsoons and (b) driest three monsoons, the June 300 HPa height anomalies for (c) the wettest three monsoons and (d) driest three monsoons, and the June total precipitable water anomalies for (e) the wettest three monsoons and (f) the driest three monsoons. The average used in the difference is for the 9 years that are not considered wet or dry. The grey shading denotes the t-test statistic greater than 95% confidence, comparing the anomalous years to the other 9 years.

Figure 11. June surface temperature anomalies for (a) wettest three monsoons and (b) driest three monsoons, the June 300 HPa height anomalies for (c) the wettest three monsoons and (d) driest three monsoons, and the

June total precipitable water anomalies for (e) the wettest three monsoons and (f) the driest three monsoons. The average used in the difference is for the 9 years that are not considered wet or dry. The grey shading denotes the t-test statistic greater than 95% confidence, comparing the anomalous years to the other 9 years.

Figure 12. (a) June mean (9 years not considered wet or dry) vertically integrated moisture transport and the moisture transport anomalies for (b) the wettest three monsoons and (c) driest three monsoons. The unit vector is shown, and the units are kg $(ms)^{-1}$. Colors indicate t-test statistic greater than 95% where blue indicates zonal transport, green indicates meridional transport and red indicates both components.

Figure 12. (a) June mean (9 years not considered wet or dry) vertically integrated moisture transport and the moisture transport anomalies for (b) the wettest three monsoons and (c) driest three monsoons. The unit vector is shown, and the units are kg (ms)-1. Colors indicate t-test statistic greater than 95% where blue indicates zonal transport, green indicates meridional transport and red indicates both components.

Figure 13. Time series of percent of WMX precipitation from (a) MX, (b) BO, (c) Tat and (d) NPa source regions. The solid line indicates the average of all fifteen years of the simulation, the long dash line indicates average over the three wettest years and the short dash line indicates average over the three driest years.

Figure 13. Time series of percent of WMX precipitation from (a) MX, (b) BO, (c) Tat and (d) NPa source regions. The solid line indicates the average of all fifteen years of the simulation, the long dash line indicates average over the three wettest years and the short dash line indicates average over the three driest years.

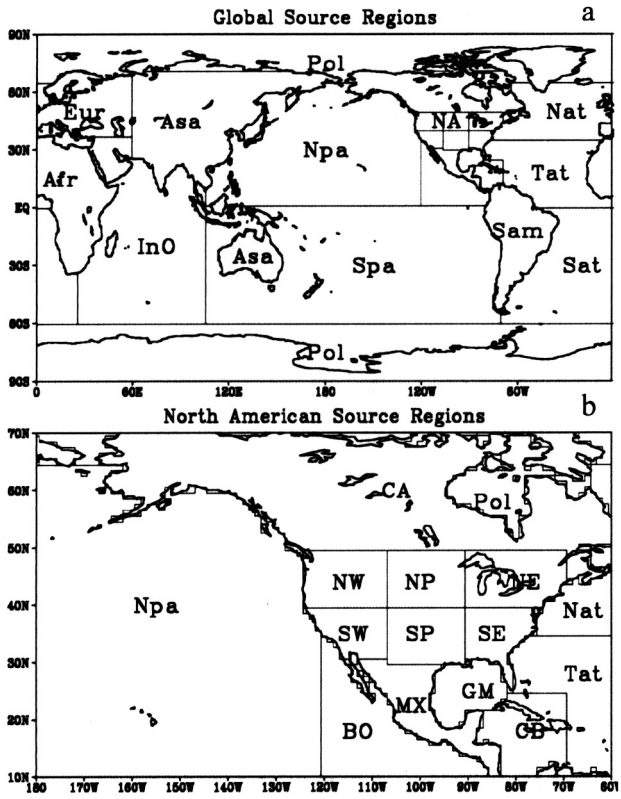

Figure 1. Map showing (a) the large-scale continental and oceanic sources of water, and (b) the North American regional sources of water. The large-scale sources are NPa – north Pacific Ocean, Spa – south Pacific Ocean, Sat – south Atlantic Ocean, InO – Indian Ocean, Tat – Tropical Atlantic Ocean, Nat – north Atlantic Ocean, Eur – Europe, Asa – Asia and Australia, Sam – South America, Afr – Africa and Pol – Polar. The regional sources are SE – South East, SP – Southern Plains, SW – South West, NW – North West, NP – Norhtern Plains, NE – North East, CA – Canada, MX – Mexico, BO – Baja Oceanic, CB – Caribbean Sea, and GM – Gulf of Mexico.

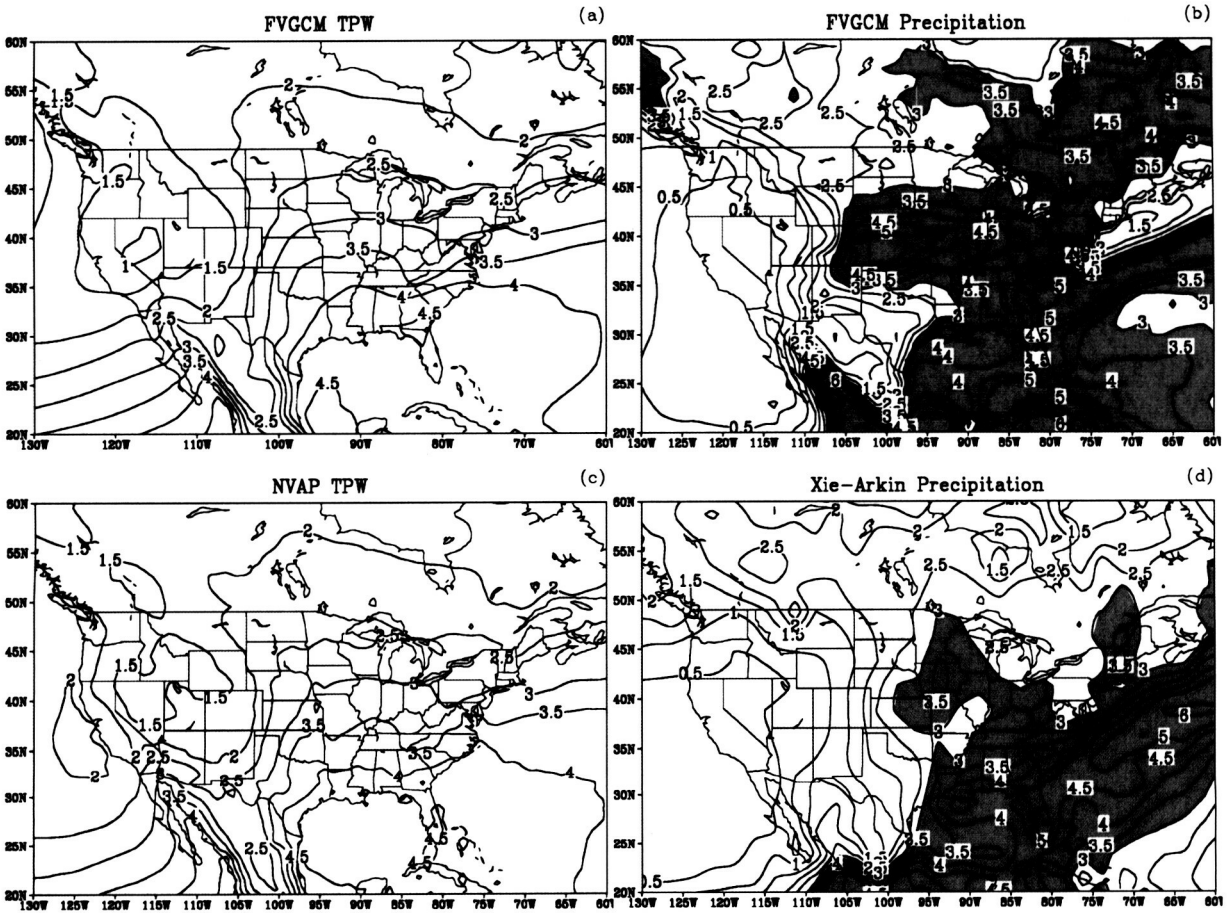

Figure 2. Summer mean (June, July and August) comparison of simulated hydrologic data with observations for FVGCM total precipitable water (cm) (a), precipitation (mm day^{-1}) (b) and observed total precipitable water (c) and observed precipitation (d). TPW observations are from NASA's Water Vapor Project (NVAP; Simpson et al. 2001) for the period 1988 - 1993 and precipitation observations are from Xie and Arkin (1997) for the period 1986-1998. Only model data that overlaps existing observations are included in (a) and (b).

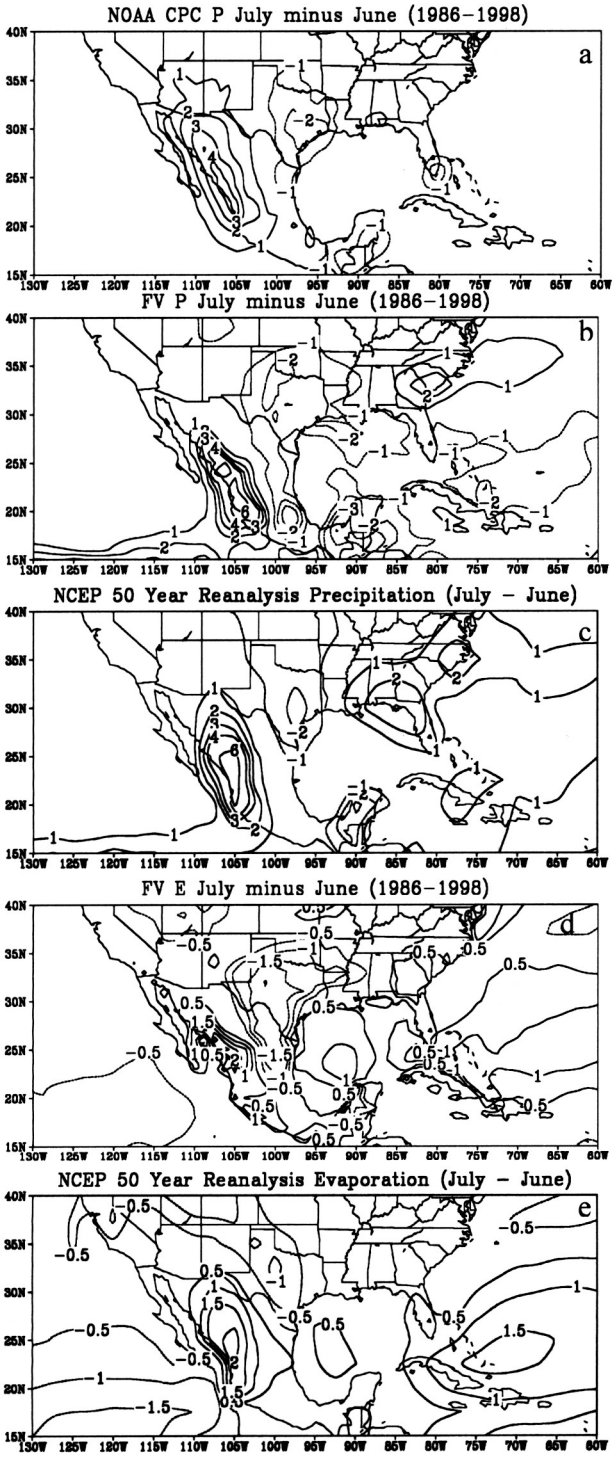

Figure 3. Difference of June and July monthly means for (a) NCDC gage precipitation (*Higgins et al.* [1996]), (b) FVGCM precipitation, (c) NCEP reanalysis precipitation, (d) FVGCM surface evaporation and (e) NCAR reanalysis evaporation. Units are mm day^{-1}. The FVGCM data are for times overlapping the NCDC available data, while NCAR reanalysis are climate averages for the 50-year reanalysis.

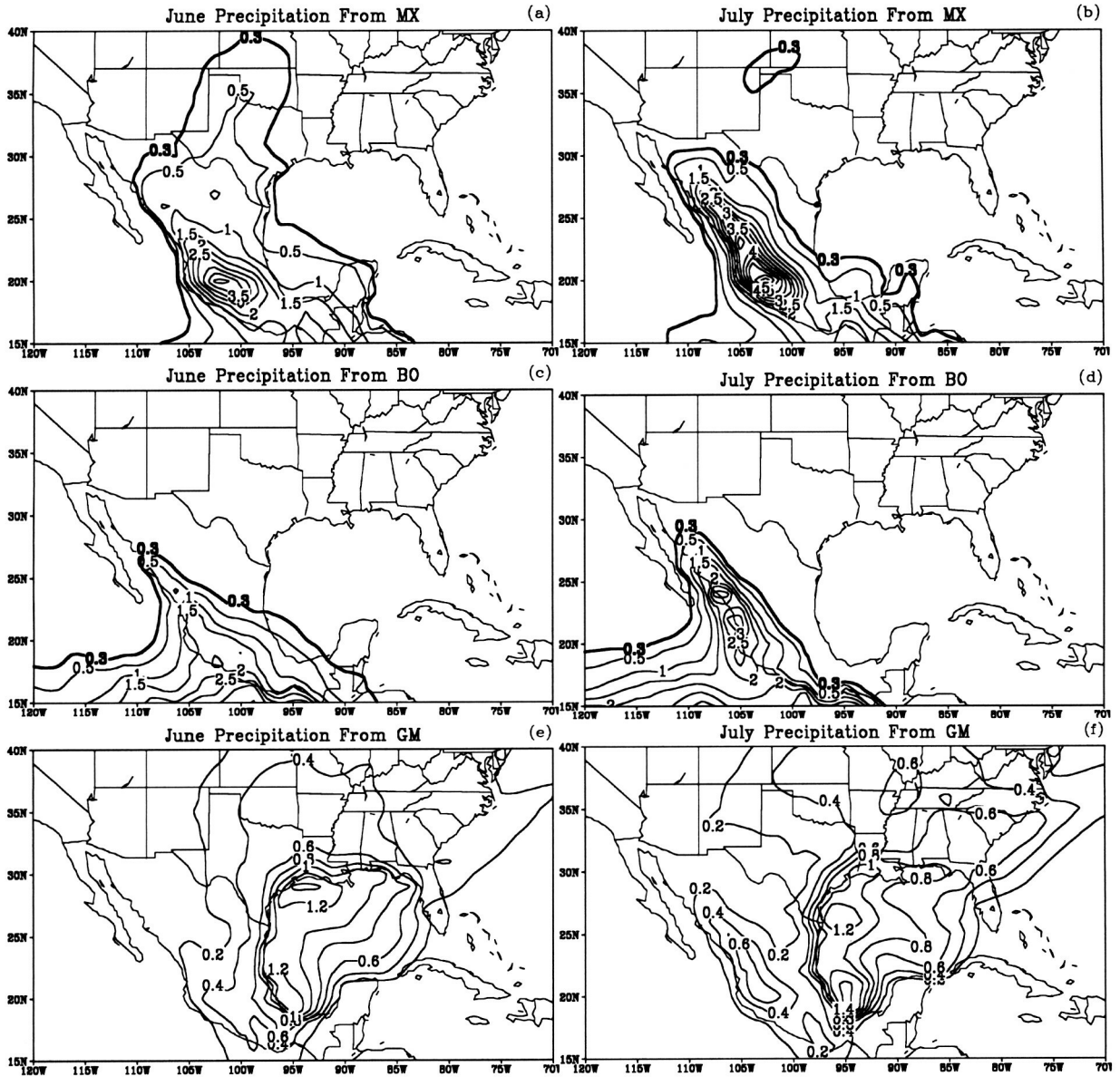

Figure 4. Precipitation that occurs from MX evaporation in (a) June and (b) July, from BO evaporation in (c) June and (d) July and from GM evaporation in (e) June and (f) July. Units are mm day^{-1}. (a) – (d) are contoured every 0.5 mm day^{-1} with an extra 0.3 mm day^{-1} contour in bold. (e) and (f) are contoured every 0.2 mm day^{-1}.

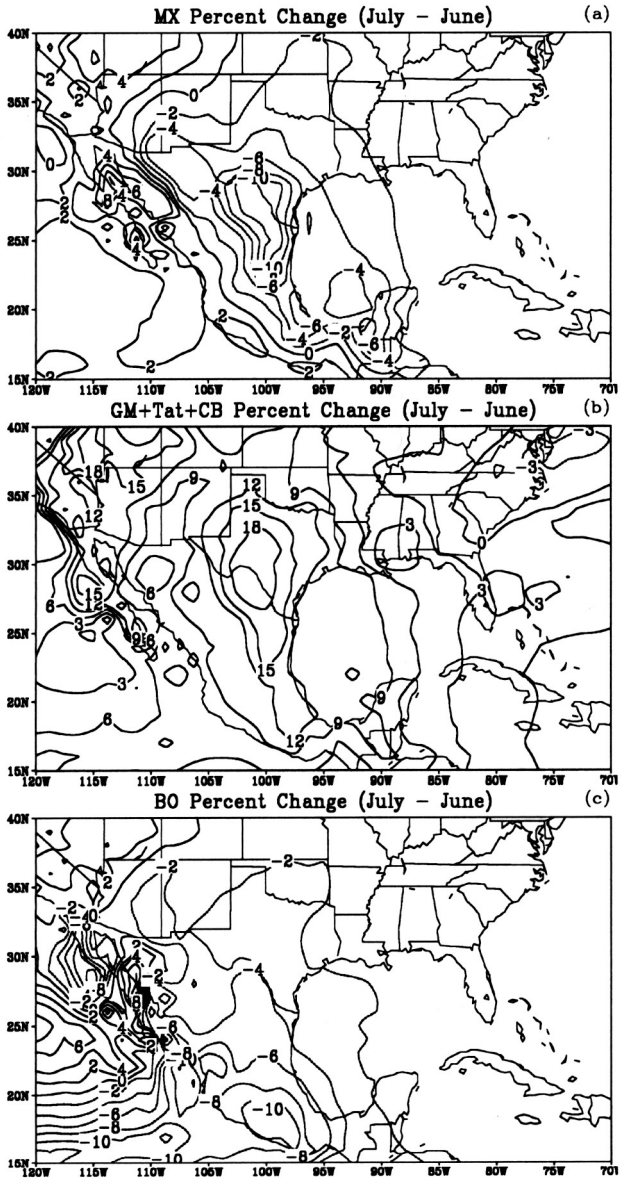

Figure 5. Difference, from June to July, of percent contribution of WVTs to total precipitation for (a) MX, (b) the sum of GM, Tat and CB, and (c) BO. The percent contribution for each WVT is computed as the sum of monthly ratio over all years.

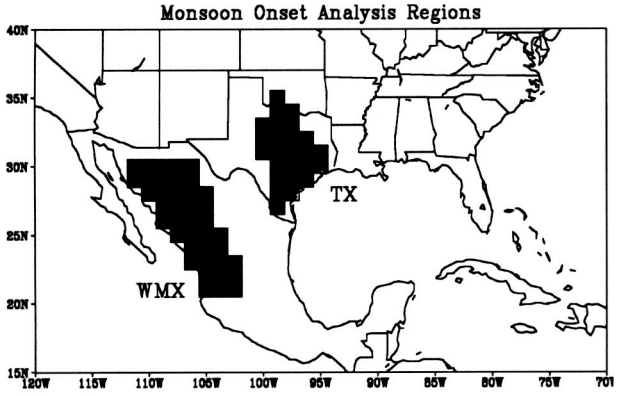

Figure 6. Map indicating the area where data are averaged for the western Mexico (WMX) and Texas (TX) regions.

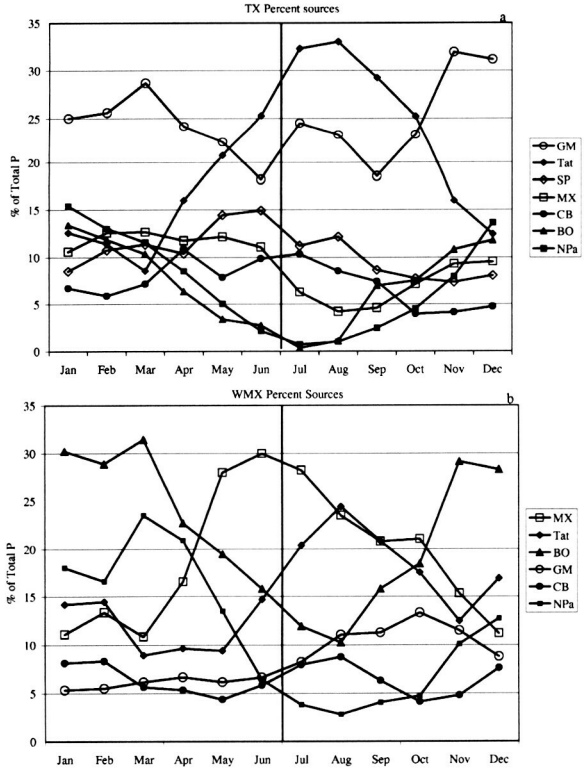

Figure 7. Mean annual cycles of the percent contribution of major source regions for precipitation in (a) TX and (b) WMX. Percentages are computed for each month of the simulation then time averaged.

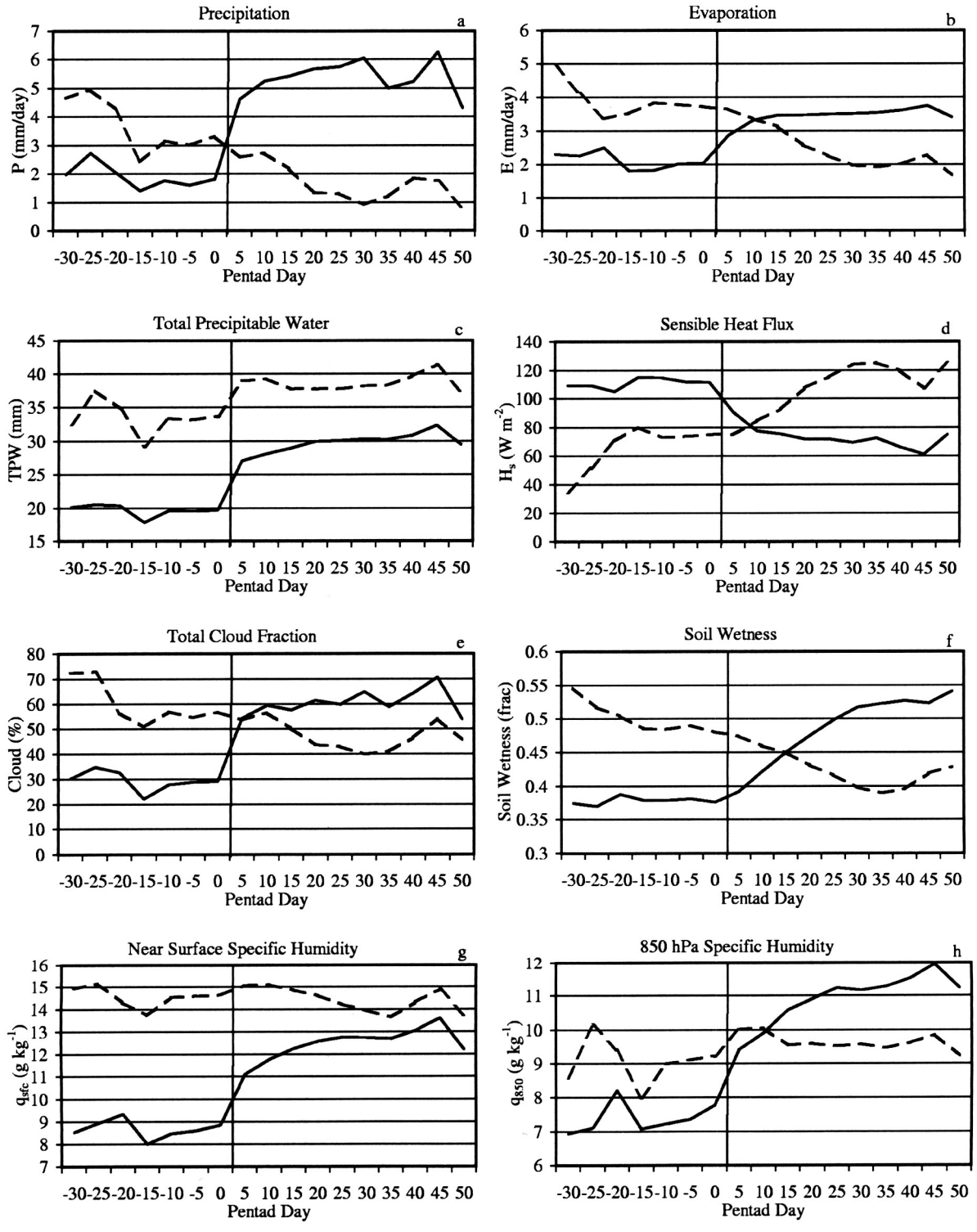

Figure 8. Composite of pentad data around the onset of heavy precipitation in WMX. The solid curve indicates WMX, and the dashed curve indicates TX. The solid vertical line indicates the time of monsoon onset in WMX.

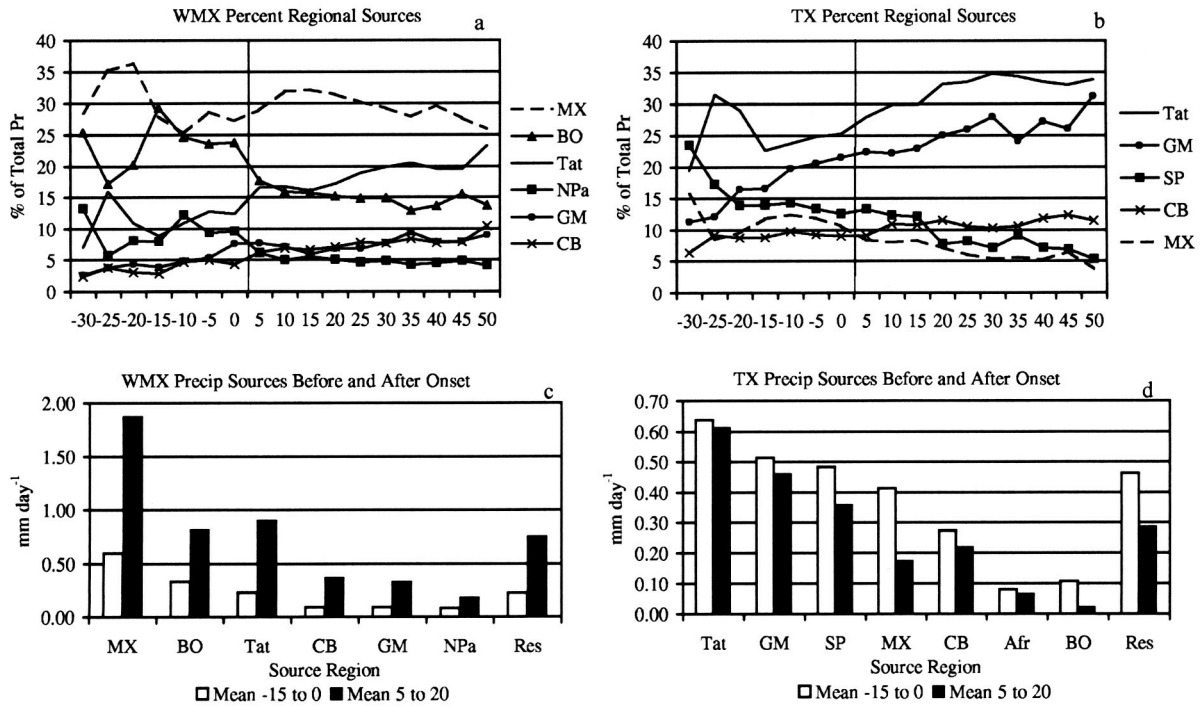

Figure 9. WVT data before and after WMX monsoon onset. Composite time series of percent of total precipitation for the major water sources in (a) WMX and (b) TX. WVT precipitation amounts of the major water sources before and after WMX monsoon onset for (c) WMX and (d) TX.

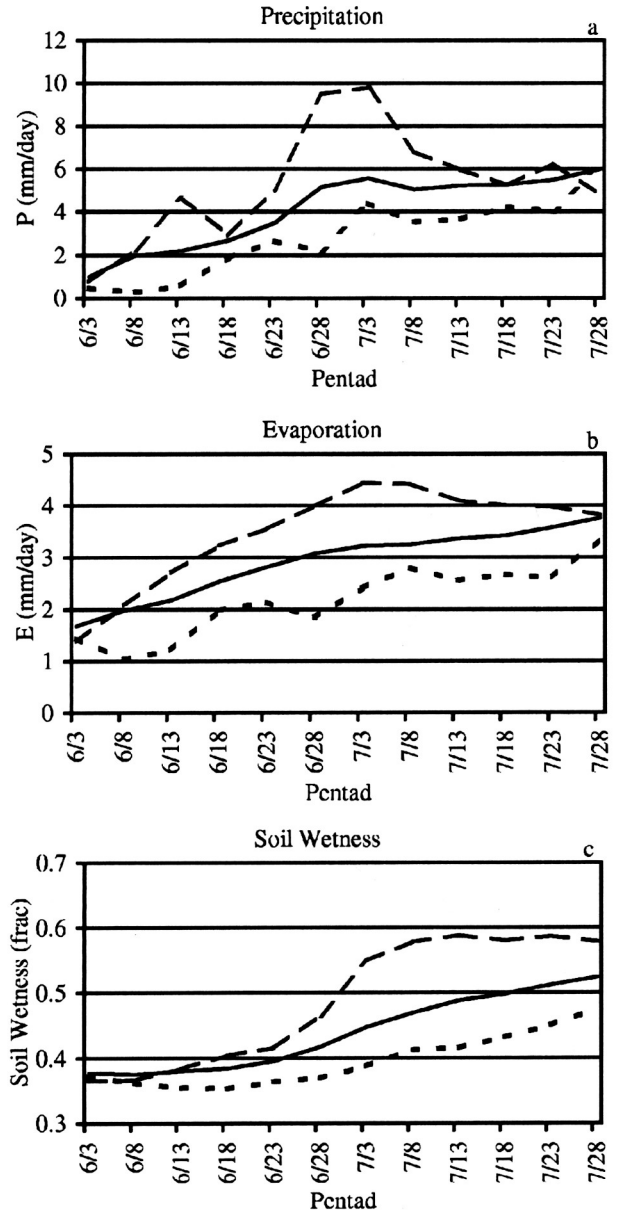

Figure 10. Time series of pentad average (a) precipitation, (b) evaporation and (c) soil wetness (fraction of saturation). The solid line indicates the average of all fifteen years of the simulation, the long dash line indicates average over the three wettest years and the short dash line indicates average over the three driest years

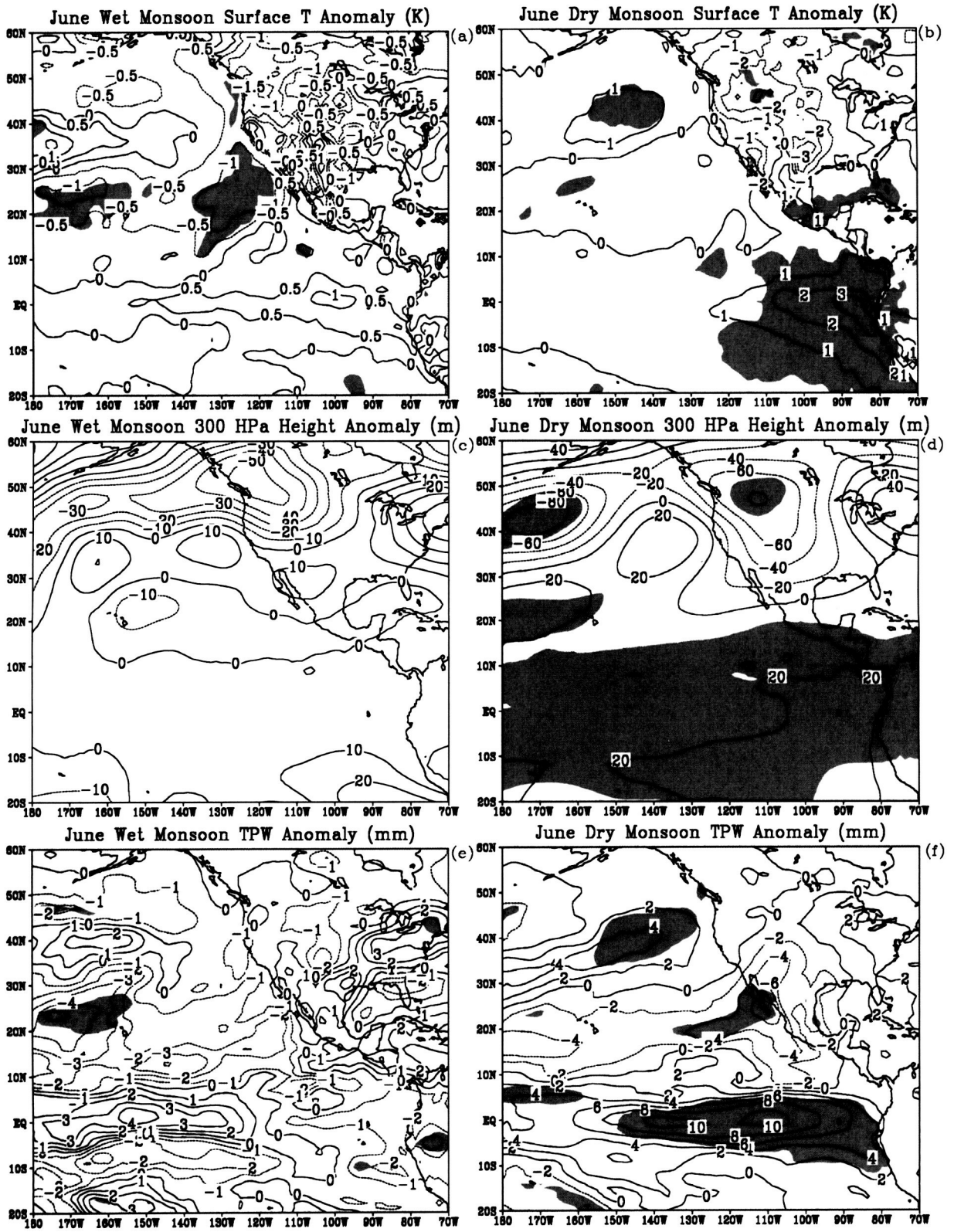

Figure 11. June surface temperature anomalies for (a) wettest three monsoons and (b) driest three monsoons, the June 300 HPa height anomalies for (c) the wettest three monsoons and (d) driest three monsoons, and the June total precipitable water anomalies for (e) the wettest three monsoons and (f) the driest three monsoons. The average used in the difference is for the 9 years that are not considered wet or dry. The grey shading denotes the t-test statistic greater than 95% confidence, comparing the anomalous years to the other 9 years.

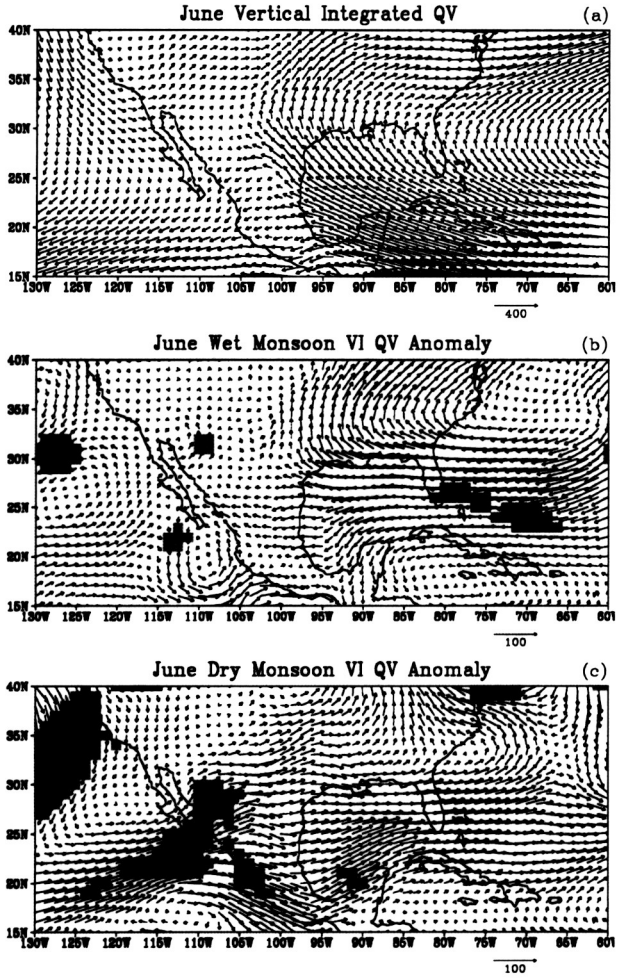

Figure 12. (a) June mean (9 years not considered wet or dry) vertically integrated moisture transport and the moisture transport anomalies for (b) the wettest three monsoons and (c) driest three monsoons. The unit vector is shown, and the units are kg $(ms)^{-1}$. Colors indicate t-test statistic greater than 95% where blue indicates zonal transport, green indicates meridional transport and red indicates both components.

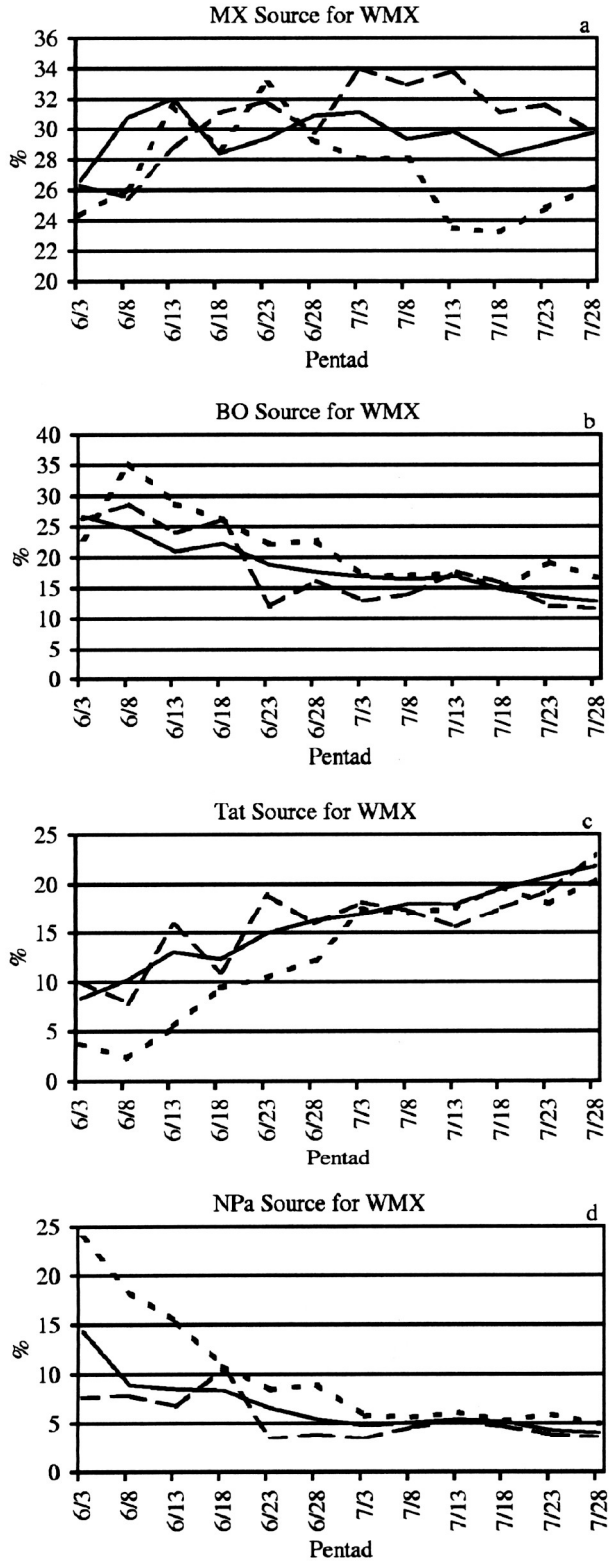

Figure 13. Time series of percent of WMX precipitation from (a) MX, (b) BO, (c) Tat and (d) NPa source regions. The solid line indicates the average of all fifteen years of the simulation, the long dash line indicates average over the three wettest years and the short dash line indicates average over the three driest years.

Popular Summary for "Numerical simulation of the large-scale North American monsoon water sources" by Michael G. Bosilovich, Yogesh C. Sud, Siegfried D. Schubert and Gregory K. Walker

The North American monsoon begins in late June or early July, and constitutes the majority of precipitation that occurs in western Mexico and the southwestern United States. In addition, it influences the atmospheric circulation and precipitation pattern in the central United States. In the published literature, there has been much discussion regarding the source(s) of water for the monsoonal precipitation (Gulf of Mexico or eastern Pacific Ocean). Understanding the sources of water can provide valuable information on the atmospheric circulation and physical processes the initiate and maintain the monsoon circulation.

In the present study, we use a global atmospheric numerical model (called a General Circulation Model, GCM) to simulate the global circulation for 15 years. Within the model, we have implemented diagnostics that follow water from its geographical source (as evaporation) to its destination (as precipitation). These diagnostics (termed Water Vapor Tracers, WVT) provide quantitative evaluation of the geographical sources of water for precipitation. Validation of the model against observations of precipitation and total water show that the model can reproduce key aspects of the monsoonal circulation. Specifically, the simulated precipitation increases dramatically in Mexico between June and July, while the precipitation in the central United States decreases.

In the central United States, surface evaporation decreases and the local sources of precipitation decrease (from June to July). On the other hand, sources of precipitation from the tropical Atlantic Ocean increase. In western Mexico (the monsoon region), local (continental) regions are important sources of precipitation before and after the monsoon onset. Sources of water from the Pacific Ocean are important to precipitation in Mexico before the monsoon onset, and do make a significant contribution after onset. However, the tropical Atlantic Ocean sources of precipitation are the most important oceanic regions to the monsoon, after onset.

Given that continental sources of precipitation are the most significant source of water to the monsoon in Mexico, we evaluated the intensity of the monsoon precipitation and surface water content leading up to the monsoon. The magnitude of surface water was not a good predictor of the intensity of the monsoon. Rather, warm sea surface temperatures (associated with El Nino) lead to less intense monsoons (which follows observations). The wettest monsoons occurred under variable conditions. However, the most intense monsoons did have large local continental sources of precipitation, while less intense monsoons were more associated with more sources of water from the Pacific Ocean and less water from the local continental sources. This study characterizes the relationship of local continental sources of precipitation (and therefore land surface processes) to the onset and maintenance of monsoon precipitation.